© 2017. Published by The Company of Biologists Ltd | Development (2017) 144, 664-676 doi:10.1242/dev.143974

RESEARCH ARTICLE

PAPC couples the segmentation clock to somite morphogenesis by regulating N-cadherin-dependent adhesion

Jérome Chal[1,2,3,4,5,*], Charlène Guillot[3,4,*] and Olivier Pourquié[1,2,3,4,5,6,7,‡]

ABSTRACT

Vertebrate segmentation is characterized by the periodic formation of epithelial somites from the mesenchymal presomitic mesoderm (PSM). How the rhythmic signaling pulse delivered by the segmentation clock is translated into the periodic morphogenesis of somites remains poorly understood. Here, we focused on the role of paraxial protocadherin (*PAPC*/*Pcdh8*) in this process. We showed that in chicken and mouse embryos, *PAPC* expression is tightly regulated by the clock and wavefront system in the posterior PSM. We observed that PAPC exhibits a striking complementary pattern to N-cadherin (CDH2), marking the interface of the future somite boundary in the anterior PSM. Gain and loss of function of *PAPC* in chicken embryos disrupted somite segmentation by altering the CDH2-dependent epithelialization of PSM cells. Our data suggest that clathrin-mediated endocytosis is increased in PAPC-expressing cells, subsequently affecting CDH2 internalization in the anterior compartment of the future somite. This in turn generates a differential adhesion interface, allowing formation of the acellular fissure that defines the somite boundary. Thus, periodic expression of PAPC in the anterior PSM triggers rhythmic endocytosis of CDH2, allowing for segmental de-adhesion and individualization of somites.

KEY WORDS: Somitogenesis, Tissue morphogenesis, Cell adhesion, Cadherin, Protocadherin, Paraxial mesoderm, Boundary formation, Endocytosis

INTRODUCTION

Somitogenesis is an early developmental process whereby pairs of epithelial spheres, called somites, form periodically from the mesenchymal presomitic mesoderm (PSM). The periodic arrangement of somites reflects the initial metameric organization of the vertebrate embryo. Somites subsequently differentiate to form the dermis, skeletal muscles and axial skeleton (Chal and Pourquie, 2009). Somitogenesis involves a molecular oscillator, called the segmentation clock, which drives the periodic expression of cyclic genes and controls coordinated pulses of Notch, fibroblast growth factor (FGF) and Wnt signaling in the PSM (Hubaud and Pourquie, 2014). These signaling pulses are thought to be translated into the periodic array of somites at a specific level of the PSM called the determination front. The determination front is defined as a signaling threshold implemented by posterior gradients of Wnt and FGF (Aulehla et al., 2003; Diez del Corral and Storey, 2004; Dubrulle et al., 2001; Hubaud and Pourquie, 2014; Sawada et al., 2001). Cells of the posterior PSM exhibit mesenchymal characteristics and express Snail-related transcription factors (Dale et al., 2006; Nieto, 2002). In the anterior PSM, cells downregulate snail/slug expression and upregulate epithelialization-promoting factors such as paraxis (Barnes et al., 1997; Sosic et al., 1997). This molecular transition correlates with the anterior PSM cells progressively acquiring epithelial characteristics (Duband et al., 1987; Martins et al., 2009). The first evidence for a segmental pattern is a stripe of expression of the transcription factors of the mesoderm posterior 2 (*Mesp2*) family, which are activated at the determination front level downstream of the clock signal. *Mesp2* expression becomes subsequently restricted to the rostral compartment of the next somite to form, where its anterior border marks the level of the future somitic boundary (Morimoto et al., 2005; Oginuma et al., 2008; Saga, 2012).

Somites are generated as a consequence of three key events. The first is the formation of the posterior epithelial wall that bridges the dorsal and ventral epithelial layers of the PSM along the future boundary and allows the formation of the somitic rosette. The second is the formation of an acellular mediolateral fissure at the level of the future boundary that separates the posterior wall of the forming somite S0 from the anterior PSM (Kulesa and Fraser, 2002; Martins et al., 2009; Watanabe and Takahashi, 2010). The third step consists of the polarization of cells of the somite's rostral compartment, which completes the epithelial rosette formation. Epithelialization of the posterior wall starts before fissure formation at the level of somite S-I (Duband et al., 1987; Pourquie and Tam, 2001; Takahashi et al., 2008). It has been shown that *Mesp2* controls the expression of the ephrin B2 receptor and *EphA4*, which promote the epithelialization of the posterior wall of the somite by downregulating Cdc42 activity (Nakajima et al., 2006; Nakaya et al., 2004; Nomura-Kitabayashi et al., 2002; Watanabe et al., 2009). In zebrafish, Ephrin-B2/EphA4 signaling in the PSM is also implicated in the activation of Integrin alpha5 at the forming somite boundary leading to the restriction of fibronectin fibril assembly in the intersomitic fissure (Koshida et al., 2005; Julich et al., 2009). The type I cadherin N-cadherin (CDH2), which is the major cadherin expressed in the paraxial mesoderm, plays an important role in somite epithelialization and boundary formation (Duband et al., 1987; Horikawa et al., 1999; Linask et al., 1998; Radice et al., 1997; McMillen et al., 2016). In zebrafish, Cdh2 is also required in adjacent PSM cells to maintain Integrin alpha 5 in an inactive conformation, thus inhibiting the formation of fibronectin fibrils inside the PSM (Julich et al., 2015). This mechanism restricts the production of the fibronectin matrix to the somitic surface and the intersomitic fissure.

[1]Stowers Institute for Medical Research, Kansas City, MO 64110, USA. [2]Development and Stem Cells, Institut de Génétique et de Biologie Moléculaire et Cellulaire (IGBMC), CNRS (UMR 7104), Inserm U964, Université de Strasbourg, Illkirch-Graffenstaden 67400, France. [3]Department of Pathology, Brigham and Women's Hospital, 77 Avenue Louis Pasteur, Boston, MA 02115, USA. [4]Department of Genetics, Harvard Medical School, 77 Avenue Louis Pasteur, Boston, MA, USA. [5]Harvard Stem Cell Institute, 77 Avenue Louis Pasteur, Boston, MA 02115, USA. [6]Anatomy and Cell Biology, University of Kansas Medical Center, Kansas City, KS 66160, USA. [7]Howard Hughes Medical Institute, Kansas City, MO 64110, USA.
*These authors contributed equally to this work

‡Author for correspondence (pourquie@genetics.med.harvard.edu)

Received 22 August 2016; Accepted 19 December 2016

Development (2017) 144, 664-676 doi:10.1242/dev.143974

Paraxial protocadherin (*PAPC*/*Pcdh8*/arcadlin) is a protocadherin implicated in paraxial mesoderm segmentation (Kim et al., 2000, 1998; Rhee et al., 2003; Yamamoto et al., 1998), in convergence-extension movements and in tissue separation during gastrulation (Hukriede et al., 2003; Kraft et al., 2012; Luu et al., 2015; Medina et al., 2004; Unterseher et al., 2004; Yamamoto et al., 2000). Also, in neurons, PAPC is involved in synapse remodeling by triggering CDH2 endocytosis (Yamagata et al., 1999; Yasuda et al., 2007). In the anterior PSM, *PAPC* is expressed in bilateral stripes under the control of the Notch/Mesp2 signaling pathway (Kim et al., 1998; Rhee et al., 2003). Interfering with PAPC function in the paraxial mesoderm in frog or mouse leads to defects in boundary formation and somite epithelialization (Kim et al., 2000; Rhee et al., 2003; Yamamoto et al., 1998). How PAPC controls somite formation is, however, not yet understood.

Here, we performed a molecular analysis of *PAPC* function during somitogenesis in chicken and mouse embryos. We show that segmental expression of PAPC downstream of the segmentation clock enhances clathrin-mediated endocytosis dynamics of CDH2, leading to somitic fissure formation through local cell de-adhesion. Thus, PAPC expression stripes in the anterior PSM establish a differential adhesion interface localized at the anterior edge of the PAPC expression domain that delimits the somite boundary.

RESULTS

PAPC expression domain defines the future somitic boundary

We isolated two distinct, full-length PAPC coding sequences from chicken embryo cDNA (accession numbers EF175382 and JN252709), resulting from the differential splicing of the 3′ end of exon 1 (Fig. 1A). Both isoforms code for transmembrane proteins composed of an extracellular domain including six extracellular cadherin (EC) motifs, a single transmembrane domain and an intracytoplasmic tail (Fig. 1A). The PAPC short isoform (PAPC-S) is lacking a 47 amino-acid stretch in its cytoplasmic domain, compared with the long isoform (PAPC-L, blue domain) (Fig. 1A). These two isoforms are similar to those described in mouse (Makarenkova et al., 2005). We next generated a polyclonal antibody against the extracellular domain of the chicken PAPC proteins. In PSM protein extracts, PAPC appears as a doublet around 110 kD, close to the predicted molecular weight of the isoforms (103 and 108 kD, respectively) with the long isoform appearing to be more abundant (Fig. 1B).

During chicken embryo development, *PAPC* mRNA expression is first detected at stage 4HH (Hamburger and Hamilton) in the newly ingressed paraxial mesoderm (data not shown). From the onset of somitogenesis (stage 7HH; day 1) to the end (stage 24HH; day 4), *PAPC* expression formed a marked, decreasing rostrocaudal gradient along the PSM, with two or three stripes in the anterior PSM (Fig. 1C-F). *PAPC* mRNA expression was observed by *in situ* hybridization in the posterior PSM, but no protein could be detected (compare Fig. 1E and 1G). In the anterior-most PSM and forming somite (S-I to SI), *PAPC* mRNA and protein were detected in a striped pattern (Fig. 1E-H). In the anterior PSM, *PAPC* mRNA expression becomes restricted to the rostral compartment of the forming somite, creating an interface at the level of the forming boundary (Fig. 1I).

The dynamic expression of PAPC is downstream of the segmentation clock

We noticed different *PAPC* expression patterns in the PSM of chicken embryos with exactly the same somite number, suggesting that *PAPC* expression is highly dynamic (Fig. 1J-L). In some embryos, *PAPC* expression extended along the posterior PSM, whereas in others, it was restricted to the anterior PSM (Fig. 1J-L). Direct comparison of *PAPC* expression with the cyclic gene lunatic fringe (*LFNG*) (McGrew et al., 1998) shows that *PAPC* expression also follows a periodic sequence (Fig. 1J-M, n=17). In contrast to *LFNG*, however, *PAPC* is never detected in the most caudal part of the PSM. During phase I of the *LFNG* cycle (Pourquie and Tam, 2001), when *LFNG* is expressed in a broad posterior domain, *PAPC* is also expressed in a broad, gradient-like domain in the posterior PSM (Fig. 1J). As the *LFNG* expression domain moves and narrows anteriorly, the *PAPC* expression domain likewise becomes restricted to the anterior PSM (Fig. 1K-M). This dynamic expression in the posterior PSM suggests that *PAPC* defines a new class of cyclic gene regulated by the segmentation clock (Fig. 1M).

Because the segmentation clock is mainly regulated by FGF, Wnt and Notch signaling, we next explored the role of these signaling pathways in regulating *PAPC* dynamic expression. Strikingly, compared with FGF signaling gene targets, *PAPC* exhibits a reverse expression gradient (decreasing caudally) in the PSM. We tested whether *PAPC* expression in the posterior PSM is regulated by FGF signaling, using SU5402, a FGF signaling inhibitor (Mohammadi et al., 1997). In treated embryos, *PAPC* expression was strongly upregulated throughout the PSM compared with control DMSO-treated embryos (Fig. 2A,B; n=7) indicating that FGF signaling represses *PAPC* expression in the posterior PSM. Mesogenin 1, a transcription factor expressed in the posterior PSM downstream of Wnt signaling, plays a key role in paraxial mesoderm patterning in the mouse embryo (Buchberger et al., 2000; Wittler et al., 2007; Yoon and Wold, 2000). Overexpression by electroporation of the chicken mesogenin 1 homolog *MESPO* (Buchberger et al., 2000) in the PSM resulted in strong ectopic expression of *PAPC* throughout the paraxial mesoderm, except in the most caudal region (Fig. 2E,F; n=9). These data suggest that a periodic FGF input inhibits the Wnt/mesogenin 1-dependent *PAPC* expression in the posterior PSM, resulting in the cyclic transcription of *PAPC*.

We then examined the role of Notch signaling in *PAPC* regulation in chicken embryo explants using the γ-secretase inhibitor DAPT. Treatment resulted in the complete loss of *PAPC* expression stripes in the anterior PSM (Fig. 2A,C,D; n=9). However, in the DAPT-treated embryos, *PAPC* maintained a distinct cycling expression domain in the posterior PSM (Fig. 2C,D). This suggests that *PAPC* dynamic expression in the posterior PSM does not depend on Notch signaling. Overexpression of the chicken *Mesp2* homolog (*MESO2*) by electroporation, resulted in a strong ectopic expression of *PAPC* throughout the paraxial mesoderm (Fig. 2G; n=7) compared with control embryos (Fig. 2E; n=8). Together, these data confirm that in the anterior PSM of the chicken embryo, *PAPC* becomes regulated by *Mesp2/MESO2* downstream of Notch signaling as reported in frog and mouse (Kim et al., 2000; Nomura-Kitabayashi et al., 2002; Rhee et al., 2003).

To assess whether the regulation of PAPC expression is conserved in amniotes, we re-investigated *Papc* mRNA and protein expression in mouse embryos (Makarenkova et al., 2005; Rhee et al., 2003; Yamamoto et al., 2000). We generated a polyclonal antibody against the mouse PAPC protein and observed an antigen distribution similar to that observed in the chicken paraxial mesoderm. Mouse PAPC is expressed in dynamic stripes in the anterior PSM and becomes localized in the rostral compartment of the forming somite S-I, posteriorly to the forming boundary (Fig. 1H). Although *Papc* mRNA expression is much fainter in the posterior PSM than in the anterior PSM, analysis of stage-matched

Development (2017) 144, 664-676 doi:10.1242/dev.143974

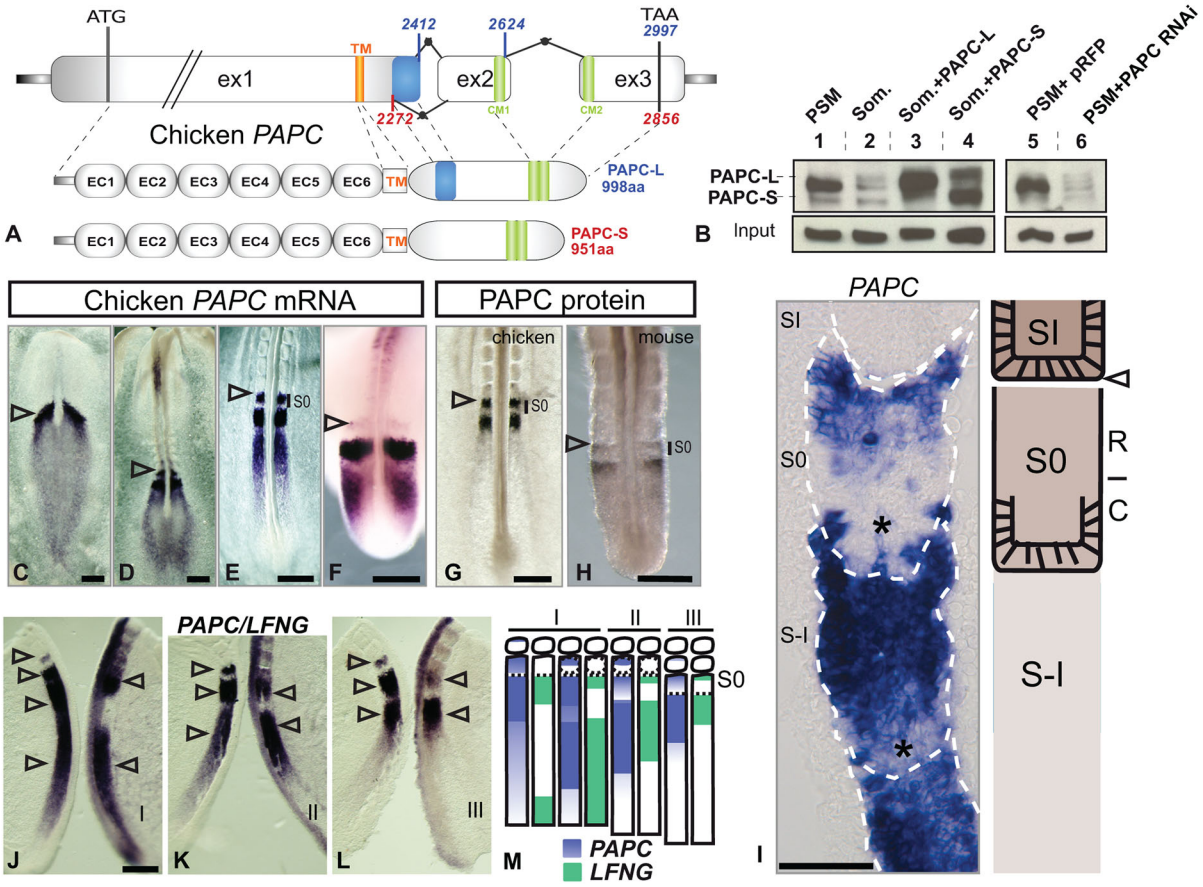

Fig. 1. Characterization of chicken paraxial protocadherin. (A) Organization of the *PAPC* locus showing sequence features (in base pairs). The long (PAPC-L) and short (PAPC-S) isoforms differ by alternative splicing of the 3′ end of exon1 (blue box). CM1/2, conserved domains of δ-protocadherins (green boxes); EC, extracellular cadherin motif; ex, exon; TM, transmembrane domain. (B) Chicken PAPC protein expression by western blot on extracts of wild-type PSM (lane 1), wild-type somite (2), somites overexpressing PAPC-L (3) or PAPC-S isoform (4), and PSM expressing *PAPC* RNAi constructs (5,6). (C-H) *PAPC* mRNA expression in chicken embryo at stage 6HH (C), 6-somite stage (D), E2 (20-somite) embryo (E), E3 embryo (F), and of PAPC protein in E2 (20-somite) chicken embryo (G), and in mouse at E10.5 (H). Whole embryo is shown in C,D and detail of the posterior region showing the PSM in E-H. S0, forming somite. Arrowheads denote the last formed somite boundary. (I) Left: parasagittal section showing chicken *PAPC* mRNA expression in the anterior PSM (blue). Somite boundaries are delimited by white dashed lines. Caudal half somites lacking *PAPC* mRNA are indicated by asterisks. Right: corresponding diagram. C, caudal; R, rostral; S-I/0/I, somite -I/0/I. Arrowhead indicates the last formed somite boundary. (J-M) Direct comparison of *PAPC* and *LFNG* mRNA dynamics on bisected E2 (20-somite) chicken embryos (J-L; *n*=17) and corresponding scheme (M). Arrowheads denote expression stripes. Segmentation clock phases are indicated by roman numerals. (C-H,J-L) Dorsal views, anterior to the top. Scale bars: 200 µm (C-H,J-L); 50 µm (I).

mouse embryos showed distinct patterns of *Papc* mRNA expression in the posterior PSM (Fig. 2H-J, arrowheads), consistent with the idea that *Papc* expression is also regulated by the segmentation clock in mouse.

We then examined *Papc* expression in several mouse lines with mutations in components of key signaling pathways involved in the segmentation clock control and PSM maturation. In *Rbpj* mutant mice, which are defective for Notch signaling (Oka et al., 1995), *Papc* expression was strongly reduced, but one or two diffuse expression stripes were nevertheless observed in a region completely lacking somites in the posterior paraxial mesoderm (Fig. 2K,L, arrowheads; *n*=13). These data suggest that, as in chicken embryos, the periodic activation of mouse *Papc* in the posterior PSM is independent of Notch signaling. The vestigial tail (*Vt*) mouse mutant is a hypomorphic mutant of *Wnt3a*, which exhibits a loss of Wnt signaling in the tail bud at embryonic day (E) 10.5 (Aulehla et al., 2003; Greco et al., 1996). In this mutant, *Papc* expression was strongly downregulated, and the expression stripes were often fused and mispatterned compared with control (Fig. 2M-O, arrowheads; *n*=5). Retinoic acid signaling has also been shown to contribute to paraxial mesoderm maturation by antagonizing the Wnt/FGF posterior gradient (Diez del Corral et al., 2003; Moreno and Kintner, 2004; Niederreither and Dolle, 2008). In *Raldh2* (*Aldh1a2*) null mutant mice, which are defective for retinoic acid production, *Papc* expression was restricted to the anterior-most PSM and formed narrow asymmetrical stripes (Fig. 2P,Q; *n*=5). As *Raldh2* mutants exhibit a FGF signaling gain-of-function phenotype in the PSM (Vermot et al., 2005), the lack of posterior expression of *PAPC* in these mutants is consistent with the FGF-dependent repression observed in chicken embryos. Thus, our data identifies *PAPC* as a novel type of cyclic gene exhibiting an unusual periodic repression in the PSM downstream of FGF signaling in the mouse and chicken embryos.

Complementary distribution of PAPC and CDH2 along the PSM

In the anterior PSM, although CDH2 is present throughout the tissue, its protein exhibits a striking segmental pattern complementary to PAPC (Fig. 3A,B). In the chicken embryo, epithelialization of the posterior somitic wall begins before the

Development (2017) 144, 664-676 doi:10.1242/dev.143974

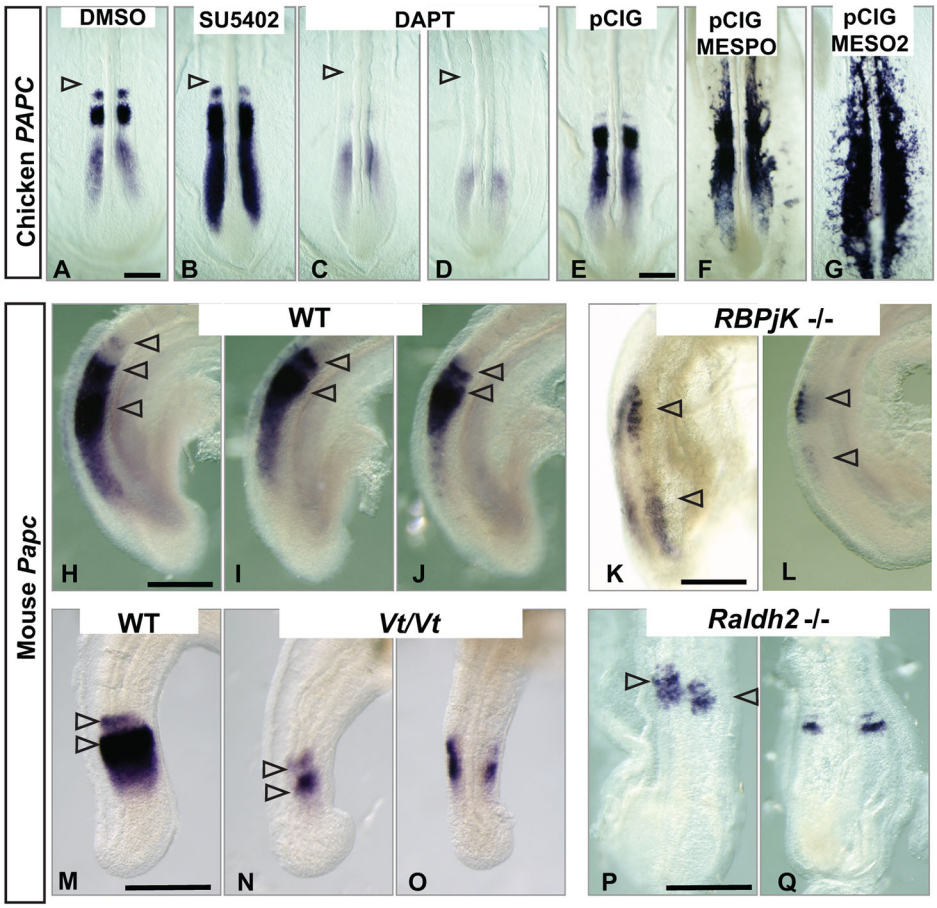

Fig. 2. The periodic expression of *PAPC* is controlled by FGF/Wnt signaling in the posterior PSM and by Notch/Mesp2 in the anterior PSM. (A-D) *PAPC* expression by *in situ* hybridization of E2 chicken embryo posterior explants cultured for 3-4 h in the presence of DMSO (0.2%; A; *n*=5), SU5402 (80 µM; B; *n*=7) or DAPT (10 µM; C,D; *n*=9). Arrowheads indicate the last formed somite. (E-G) *PAPC* expression in E2 chicken embryos overexpressing a pCIG control vector (E; *n*=8), a *MESPO*-expressing vector (F; *n*=9) or a *MESO2*-expressing vector (G; *n*=7) in the PSM. (H-J) Mouse *Papc* expression by *in situ* hybridization in the PSM of stage-matched E9.5 wild-type (WT) embryos (*n*=14). Arrowheads indicate the anterior boundary of expression stripes. (K-Q) *Papc* expression in mice mutant for *Rbpj* $^{-/-}$ (E9.0; K,L; *n*=13); in control (M; *n*=12) and vestigial tail mutants (*Vt*/*Vt*) (E10.5; N,O; *n*=5); and in *Raldh2*$^{-/-}$ mutants (E8.5; P,Q; *n*=5). Arrowheads indicate expression stripes. (H-N) Anterior to the top, lateral view; (A-G,O-Q) dorsal view. Scale bars: 200 µm.

fissure forms (Duband et al., 1987; Nakaya et al., 2004). Thus, in the forming somite (S0), the epithelialization process is more advanced in the caudal compartment than in the rostral one, as evidenced by increased colocalization of CDH2 and F-actin (Fig. 3B,F). The rostral compartment of S0 acquires an epithelial polarity and becomes recruited to the rosette soon after formation of the posterior fissure. This transition correlates with the downregulation of PAPC in the rostral compartment of the newly formed somite, and with the accumulation of CDH2 and F-actin at the apical membrane of anterior somitic cells (Fig. 3D,F). At the forming boundary level (S-I/S0), PAPC is excluded from the posterior epithelializing domain of S0 (Fig. 1I; Fig. 3C-E). In the posterior wall of S0, CDH2 was found to be essentially located at the cell membrane of epithelial cells (Fig. 3D). In contrast, in the rostral part of S-I, CDH2 and PAPC are also found intracellularly. Using the anti-PAPC polyclonal antibody and a secondary antibody labeled with gold particles, we analyzed PAPC distribution by electron microscopy in the anterior compartment of S0 and detected PAPC primarily at cell-cell contacts and sites of membrane trafficking, including clathrin pits and endocytosis vesicles (Fig. S1).

In order to evaluate CDH2 and PAPC colocalization, we performed a cross-correlation study of the intensity profile of PAPC and CDH2, which was compared with a similar analysis between CDH2 and F-actin (which colocalize in the apical domain of epithelial cells). The analysis was performed in the chicken anterior PSM (Fig. 3B,F; Fig. S2). As expected, the strongest correlation coefficient obtained was for CDH2 and F-actin in the newly formed somite (SI) where CDH2 complexes are stabilized by the network of F-actin to maintain the epithelial structure of the somite (Fig. 3F). Interestingly, we observed a graded decrease of the correlation coefficient of CDH2 and F-actin from high in somite to low in the PSM consistent with the progressive nature of the epithelialization process along the PSM (Fig. 3F; Fig. S2). The correlation between PAPC and CDH2 was maximal in the rostral part of the somite 0 (S0 R) and in the somite I (S-I) where PAPC is strongly expressed indicating that CDH2 and PAPC largely colocalize in these regions of the PSM (Fig. 3B,F).

We also performed cross-correlation measurements of the intensity profile of PAPC and CDH2 or of CDH2 and F-actin at the interface between cells in the rostral part of S0 (Fig. 3G; Fig. S2). As in the cross-correlation analysis described above, the values were compared with that obtained for F-actin and CDH2 colocalization in the somite. Interestingly, the correlation was high (correlation coefficient=0.8) with a peak of colocalization found at 0 µm indicating that PAPC and CDH2 are strongly colocalizing in the rostral part of S0, at a 200 nm resolution (Fig. 3G). These data suggest that PAPC and CDH2 are also located in close proximity at the cell membrane in the rostral compartment of S0. Attempts to co-immunoprecipitate PAPC with CDH2 from chicken PSM extracts were negative, suggesting that the PAPC and CDH2 do not directly interact (data not shown).

PAPC regulates somite boundary formation and CDH2 distribution at the cell membrane

The striking complementary patterns of PAPC and CDH2 expression during somitogenesis prompted us to examine whether PAPC interferes with CDH2 function during somitogenesis. We used *in ovo* electroporation of the primitive streak paraxial

Development (2017) 144, 664-676 doi:10.1242/dev.143974

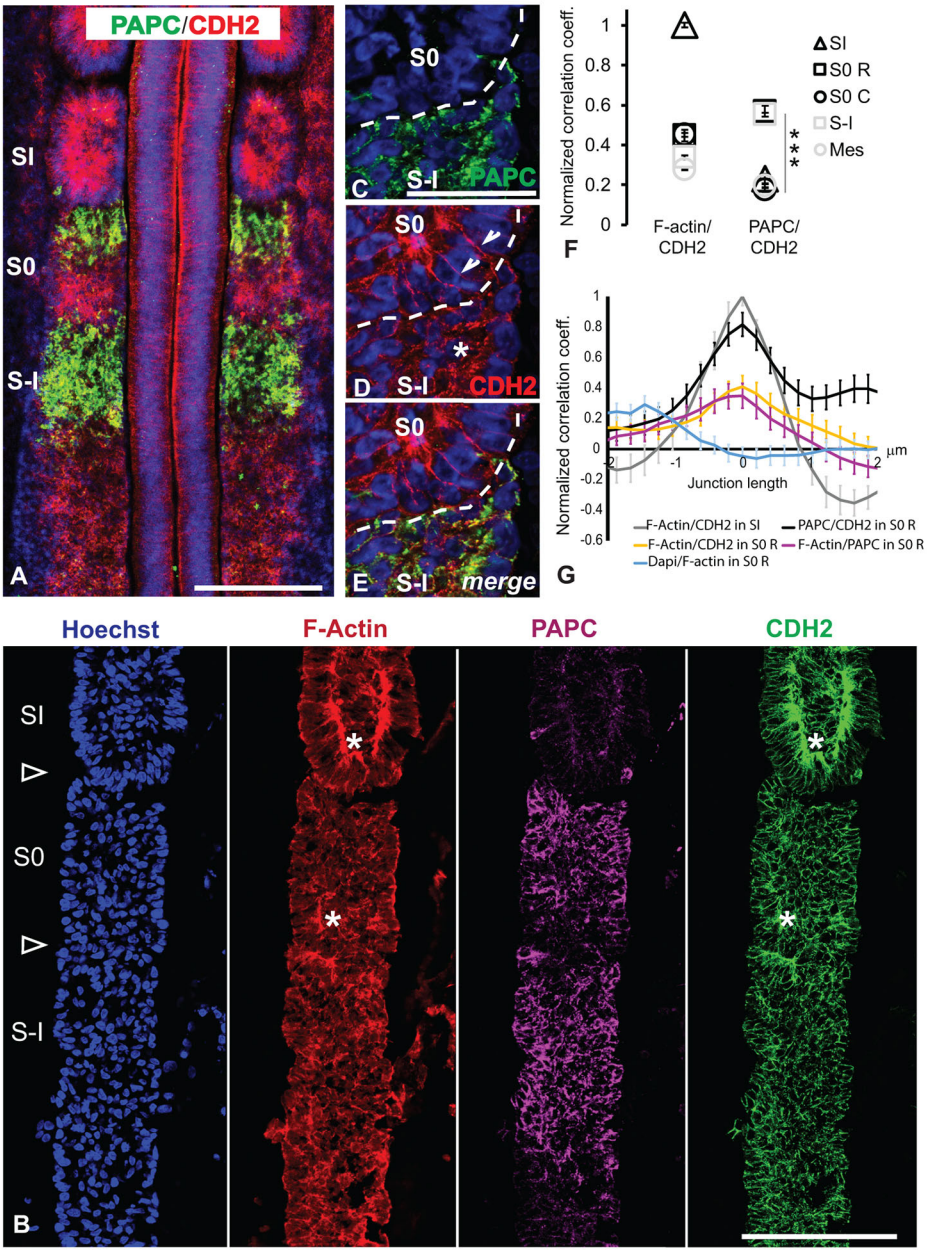

Fig. 3. Complementary distribution of PAPC and CDH2 in the forming somite. (A) Comparison of PAPC (green) and CDH2 (red) distribution by immunohistochemistry in the anterior PSM. Nuclei are labeled in blue. Dorsal view, anterior to the top. Scale bar: 200 µm. (B) Confocal images of parasagittal sections of a stage 15 somite chicken embryo PSM stained for nuclei (Hoechst, blue), F-actin (Phalloidin, red), PAPC (magenta) and CDH2 (green). Arrowheads mark somitic boundaries, asterisks mark sites of CDH2 and F-actin epithelial colocalization. Scale bar: 100 µm. (C-E) Confocal images of the interface between somites S0 and S-I, immunostained for PAPC (green) and CDH2 (red). The dashed white line marks the position of the forming boundary. Nuclei are labeled in blue. Scale bar: 50 µm. (F) PAPC, CDH2 and F-actin colocalization analysis in the anterior PSM. Normalized correlation coefficients were calculated based on signal intensity profiles for each staining within each PSM subdomains (n=3 embryos). A value of 1 corresponds to a total positive correlation. C, caudal half; mes, posterior PSM mesenchyme; R, rostral half; S-I/0/I, somite -I/0/I. ***P<0.0005. (G) PAPC, CDH2 and F-actin colocalization analysis at cellular junctions. Normalized correlation coefficients were calculated based on signal intensity profiles along cell-cell junctions in various PSM subdomains (n=20 junctions per domain; R, rostral; S0/I, somite 0/I). A value of 1 corresponds to a total positive correlation, and a peak centered at 0 µm indicates that both signals are colocalized.

mesoderm precursors to overexpress PAPC constructs in the PSM (Dubrulle et al., 2001). Chicken embryos overexpressing the long PAPC isoform (PAPC-L) were not different from control embryos overexpressing the empty vector (data not shown). In contrast, when we overexpressed the short PAPC isoform (PAPC-S) and a membrane-bound GFP reporter, electroporated cells formed clumps of cells, which interfered with proper somite morphogenesis, forming mesenchymal bridges that blocked boundary formation (Fig. 4A,B; n=25, control n=15). Also, electroporated anterior PSM and newly formed somite cells exhibited a rounder, more mesenchymal morphology, losing the apical accumulation of CDH2 (Fig. 4D-I). We also observed differential sorting of the electroporated cells, which were found preferentially in the rostral mesenchymal compartment of newly formed somites (Fig. 4M,N; n>6 per condition). In clumps of PAPC-S-overexpressing cells, CDH2 expression was only detectable at a low level at the cell membrane compared with neighboring cells and with control electroporated cells (compare Fig. 4D-F and 4G-I). Hence, overexpression of PAPC-S in anterior PSM cells reduces CDH2 distribution at the membrane of the expressing cells. CDH2 plays an important role in the maintenance of the epithelial structure in anterior PSM (Duband et al., 1987; Horikawa et al., 1999; Linask et al., 1998; Radice et al., 1997) and in boundary formation (McMillen et al., 2016). Thus, the reduction of CDH2 at the membrane of cells overexpressing PAPC could explain their loss of epithelial polarity, their acquisition of a mesenchymal fate and their segregation in the rostral compartment of the forming somite.

We then examined the effect of PAPC knockdown in anterior PSM cells. Chicken embryos electroporated with PAPC-RNAi exhibited strong downregulation of *PAPC* mRNA expression (Fig. S3), associated with a loss of PAPC protein in PAPC RNAi-expressing cells compared with controls (Fig. 1B; Fig. S3). Notably, the PAPC RNAi-expressing cells were located preferentially in the epithelial fraction of the somite, showing an opposite behavior to cells expressing PAPC-S (Fig. 4C,N; n=25). Cells in which PAPC

Development (2017) 144, 664-676 doi:10.1242/dev.143974

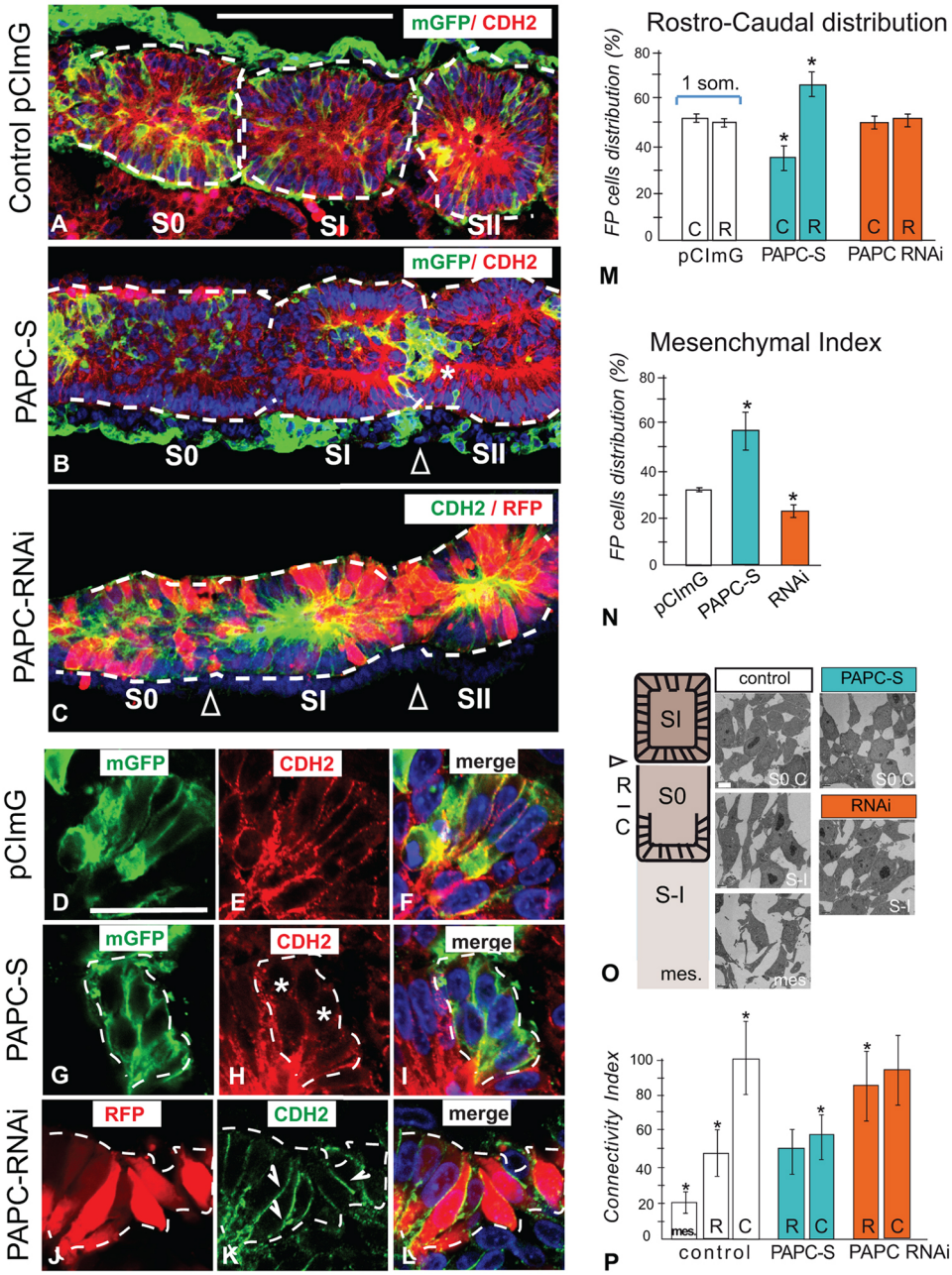

Fig. 4. *PAPC* misexpression disrupts somite boundary formation and CDH2 localization. (A-C) CDH2 immunostaining of parasagittal sections of E2 chicken embryo PSM electroporated with pCImG (control, A; *n*=15), PAPC-S (B; *n*=25) or PAPC-RNAi (C; *n*=25). Nuclei are shown in blue. Electroporated cells co-express a membrane-bound GFP (A,B,D,F,G,I, green) or cytoplasmic RFP (C,J,L, red). Somite limits are highlighted by dashed white lines. Arrowheads denote segmentation defects. Asterisk in B marks a mesenchymal clump. Scale bar: 100 µm. (D-L) Higher magnification of the newly formed somite SI of E2 chicken embryos electroporated with control pCImG (D-F), PAPC-S (G-I) and PAPC-RNAi (J-L) constructs showing immunostainings of parasagittal sections labeled with an anti-GFP (D,G, green) or an anti-RFP (J, red), and anti-CDH2 (E,H, red; K, green) and merged panels (F,I,L). Asterisks in H mark low CDH2 membrane localization in PAPC-S electroporated cells with round morphology. Arrowheads in K mark high CDH2 membrane localization in PAPC-RNAi-electroporated cells with elongated epithelial morphology. Scale bar: 25 µm. (M) Distribution of electroporated fluorescence-positive (FP) cells along the rostral (R) and caudal (C) somite compartments, in chicken embryos electroporated with pCImG, PAPC-S or PAPC-RNAi constructs (*n*>6 per condition). (N) Distribution of electroporated fluorescence-positive (FP) cells in the mesenchymal and epithelial domains (mesenchymal index) of the newly formed somites, in embryos electroporated with pCImG, PAPC-S or PAPC-RNAi constructs (*n*>6 per condition). (O) Electron microscopy analysis of cellular organization in the PSM of chicken embryos electroporated with pCImG, PAPC-S or PAPC-RNAi constructs (*n*=4 per condition). Left: PSM diagram indicating the sites of analysis, namely posterior PSM (mesenchyme, mes.), the rostral compartment of S-I (R) and the caudal compartment of S0 (C) at the level of the forming boundary. Right: representative pictures of the cellular organization of control and treated domains. Scale bar: 2 µm. (P) Cell-cell connectivity index in control embryos, and in PAPC-S- and PAPC-RNAi-electroporated embryos (*n*=4). Data shown are mean±s.e.m.; **P*<0.05; refer to Materials and Methods for quantification method.

was knocked down were preferentially located in the epithelial layer and acquired a spindle-shape morphology, accumulating CDH2 and actin cytoskeleton at their membrane (Fig. 4C,J-L,N,O). These cells formed epithelial connections between somites, interfering with proper segmentation and somite morphogenesis. No cell distribution bias along the rostrocaudal compartments of somites

Development (2017) 144, 664-676 doi:10.1242/dev.143974

was observed, possibly due to the increase in cell adhesivity (Fig. 4M). These data support the idea that PAPC activity regulates the membrane distribution of CDH2, promoting a more mesenchymal state.

We further analyzed the effect of overexpressing PAPC-S and PAPC-RNAi constructs on the cytoarchitecture of paraxial mesoderm cells by electron microscopy (Fig. 4O). A clear transition was observed on both sides of the future somitic boundary, between the mesenchymal nature of S-I and the epithelial organization of the posterior wall of S0 (Fig. 4O). The progressive epithelialization of the anterior PSM was characterized by a large increase in cell-cell connectivity, namely an increase in the number of cell-cell contacts and their length (Fig. 4O,P). Overexpression of PAPC-S resulted in a significant decrease in cell-cell connectivity in the caudal compartment of S0 compared with control (Fig. 4O,P; n=4). Conversely, expression of PAPC-RNAi constructs in the anterior compartment of S-I resulted in an increase of cell connectivity (Fig. 4O,P; n=4). This suggests that the expression level of PAPC in PSM cells is inversely correlated with their epithelialization status.

To determine whether PAPC antagonizes CDH2 function, we attempted to rescue the PAPC-S overexpression phenotype by co-electroporating a CDH2-expressing construct. However, direct expression of CDH2 in the epiblast leads to cell-sorting defects during gastrulation, thus preventing the analysis of the PSM phenotypes (data not shown). To circumvent this, we used an inducible system to restrict overexpression of CDH2 once the cells entered the PSM. The phenotype of chicken embryos overexpressing only CDH2 in the anterior PSM resembled that of PAPC loss of function with overexpressing cells clustering and integrating the epithelial compartment of the anterior PSM (Fig. 5A-H; n=25). In these embryos, intersomitic fissures were often absent as cells remained connected by epithelial bridges (Fig. 5E). Co-electroporation of the inducible CDH2 construct together with PAPC-S led to a partial rescue of somite morphogenesis (Fig. 5I; n=32). In these embryos, somite morphology was partially restored, and co-electroporated cells contributed both to the somite epithelial ring and to the mesenchymal somitocoele compartment (Fig. 5I-M). These experiments suggest that PAPC can antagonize the epithelialization-promoting function of CDH2 in the anterior PSM.

PAPC regulates endocytosis in the anterior compartment of the forming somite

Our data show that interfering with PAPC level alters the epithelial state of PSM cells and the amount of CDH2 at the cell membrane. Interestingly, in the rat nervous system, PAPC/arcadlin was shown to regulate CDH2 function by controlling its endocytosis (Yasuda

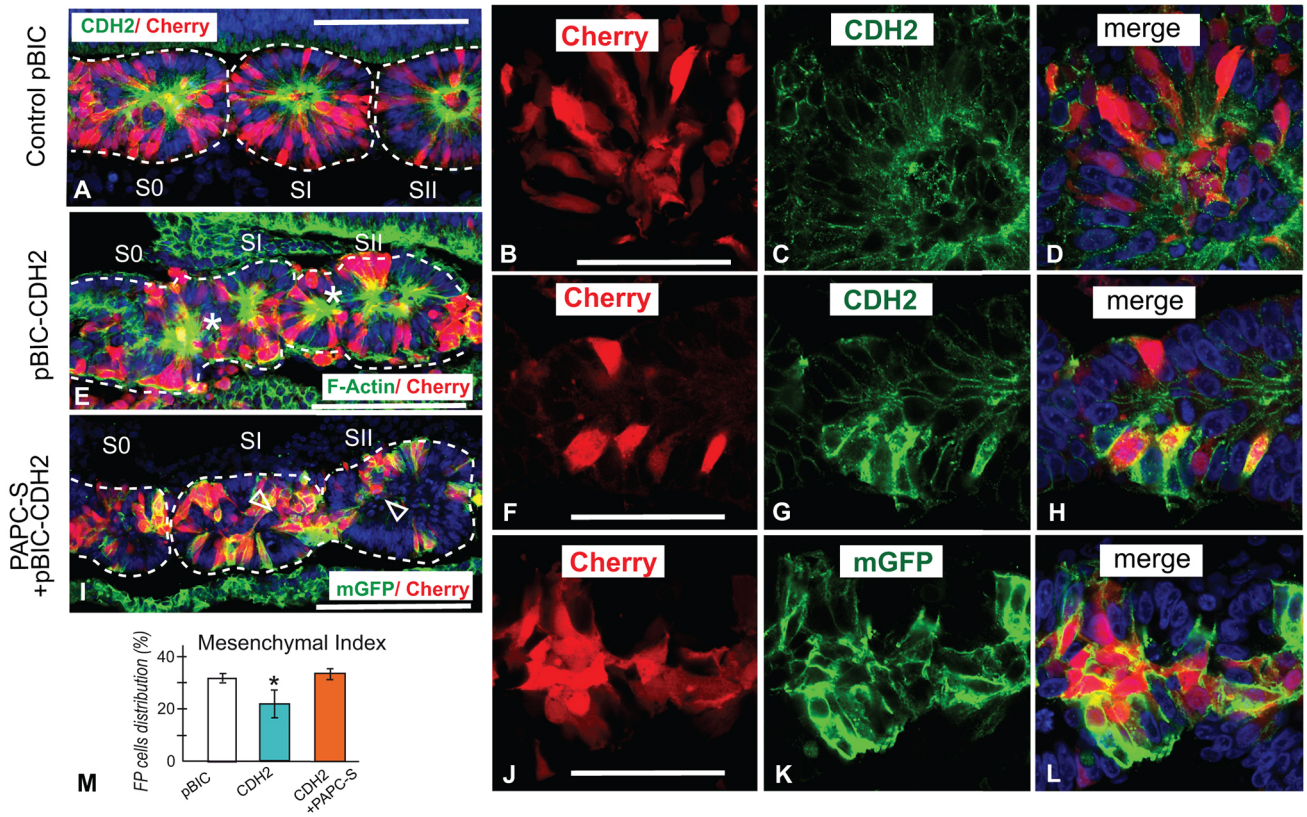

Fig. 5. PAPC negatively regulates CDH2 during somite morphogenesis. (A-L) Immunostainings of parasagittal sections of E2 chicken embryos PSM electroporated with pBIC (control; A-D; n=10), pBIC-CDH2 (E-H; n=25), or co-electroporated with pBIC-CDH2 and pCImG-PAPC-S (I-L; n=32). Electroporated cells with pBIC vectors co-express mCherry (red), and with pCImG vector co-express membrane-bound GFP (green, I-L). Nuclei are shown in blue in A,E,I and D, H,L. Somite individualization is highlighted by dashed white lines. (A,E,I) Low magnification images. Scale bars: 100 µm. Asterisks in E mark ectopic epithelial rosettes. Arrowheads in I mark contribution to somitocoele. (B-D,F-H,J-L) Higher magnification of parasagittal cryosections of the forming somite region of E2 chicken embryos electroporated with pBIC (B-D), pBIC-CDH2 (F-H) or pBIC-CDH2+pCImG PAPC-S (J-L) showing immunostainings labeled with an anti-Cherry (red, B,F,J), an anti-CDH2 (green, C,G), an anti-mGFP (green, K) and merged panels (D,H,L). Scale bars: 25 µm. (M) Distribution of electroporated fluorescence-positive (FP) cells in the mesenchymal and epithelial domains (mesenchymal index) of the newly formed somites electroporated with pBIC, pBIC-CDH2 or co-electroporated with pBIC-CDH2+pCImG PAPC-S (n>6 per condition). Mean±s.e.m. *P<0.05.

Development (2017) 144, 664-676 doi:10.1242/dev.143974

et al., 2007). Because the main pathway involved in cadherin endocytosis is the clathrin-mediated endocytosis pathway (Delva and Kowalczyk, 2009), this led us to ask whether PAPC regulates CDH2 distribution by regulating clathrin-dependent endocytosis in the chicken paraxial mesoderm. Interestingly, the rostral compartment of S-I, which strongly expresses PAPC, shows high levels of punctate clathrin staining, suggesting more active endocytosis compared with the newly formed somite S0 (Fig. 6A-F). In the rostral compartment of S-I, PAPC and CDH2 distribution largely overlaps with clathrin (Fig. 6G-L).

In order to test whether PAPC can stimulate clathrin-dependent endocytosis, we compared the uptake of fluorescent dextran in chicken embryos electroporated with a vector driving expression of PAPC-S and of a membrane-bound myristylated GFP (mGFP) or electroporated with a vector driving only expression of mGFP (pCimG) (Fig. 7A,B; Fig. S4). PAPC levels were quantified by immunohistochemistry and compared with dextran fluorescence in GFP-positive and GFP-negative cells (Fig. 7A,B; Fig. S4). As expected, the ratio of PAPC over dextran fluorescence intensity was found to be increased in cells overexpressing the PAPC-S construct. These cells also exhibited an increase in intracellular dextran fluorescence (Fig. 7A,B; Fig. S4). Treating the electroporated embryos with Pitstop2 (an inhibitor of clathrin-mediated endocytosis), prior to the addition of dextran, significantly decreased the uptake of dextran in PAPC-S-overexpressing cells (Fig. 7B; Fig. S4). Interestingly, when we compared the internalization efficiency of mGFP (internalization of which is not exclusively clathrin dependent) with that of CDH2 (which is clathrin dependent), we observed that PAPC-S-overexpressing cells specifically increase CDH2 uptake compared with cells electroporated with mGFP. Together, this suggests that PAPC specifically promotes the internalization of the clathrin-dependent dextran and CDH2 cargos (Fig. S4). Altogether, these experiments show that PAPC expression level can regulate clathrin-mediated endocytosis in anterior PSM cells.

The data above suggest that inhibiting the clathrin-mediated endocytosis pathway on a short timescale is sufficient to destabilize the dynamics of CDH2 internalization in anterior PSM cells. We next tested the role of long-term inhibition of clathrin-mediated endocytosis in somite boundary formation by treating cultured embryo explants with the endocytosis inhibitor chlorpromazine for 3-5 h. Whereas control explants formed several somites (Fig. 7C,E), treated explants did not form any new somites (Fig. 7D,F; n=7). In treated explants, PSM cells failed to adopt an elongated polarized

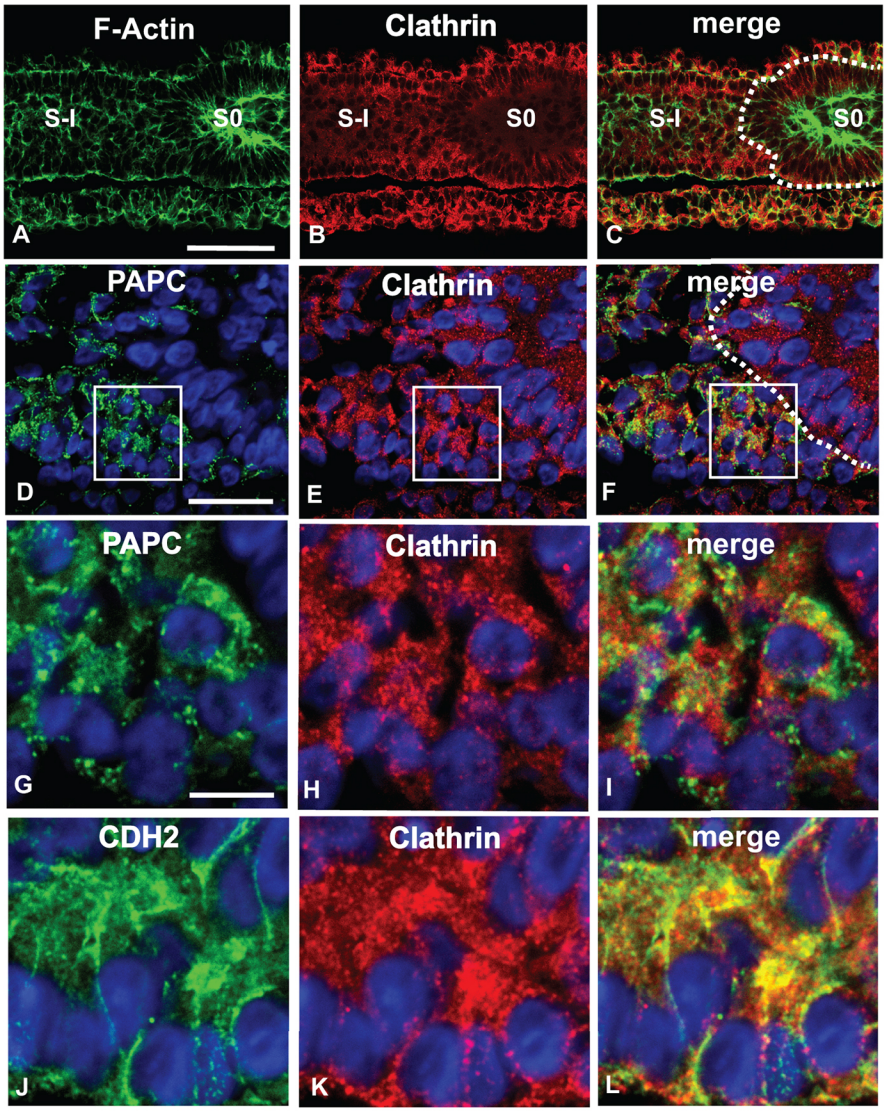

Fig. 6. PAPC, CDH2 and clathrin colocalize in the anterior PSM. (A-C) Immunostainings of parasagittal sections of E2 chicken embryos anterior PSM stained with Phalloidin (F-actin; A, green) and an antibody against clathrin (B, red) (n=4). S-I/0, somite -I/0. Scale bar: 50 µm. (D-L) Higher resolution images comparing clathrin localization with PAPC (D-I) and CDH2 (J-L) protein immunolocalization during somite formation. G-I show higher magnifications of the boxed areas in D-F, respectively. Nuclei are counterstained (blue). Parasagittal sections, anterior to the right. Scale bars: 20 µm (D-F); 10 µm (G-L).

Development (2017) 144, 664-676 doi:10.1242/dev.143974

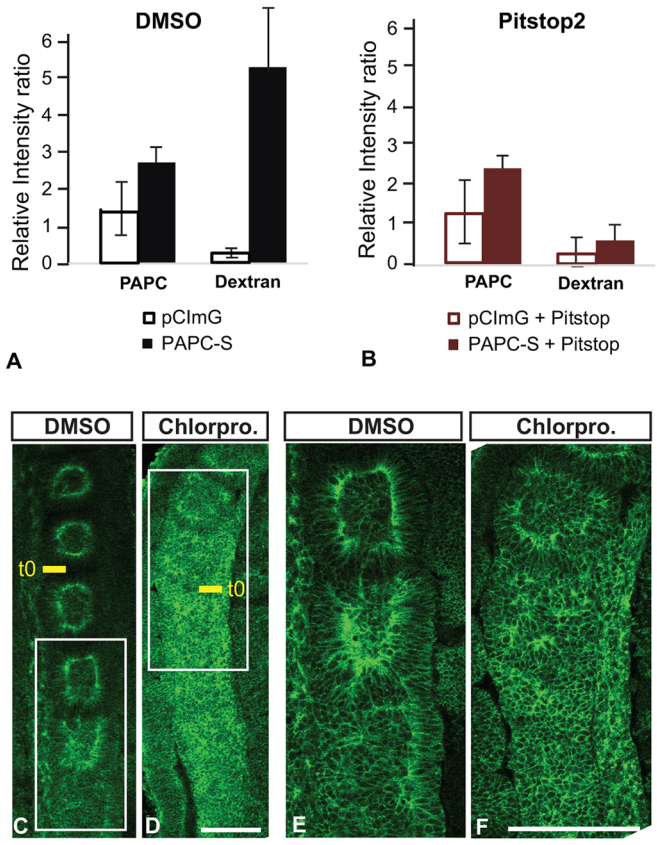

Fig. 7. PAPC promote anterior PSM cells endocytic activity. (A,B) Quantification of dextran uptake as a measure of endocytosis level. Fluorescence intensities for PAPC and dextran were measured in embryos electroporated with pCImG (white) or PAPC-S (black) and subsequently treated with DMSO (control) or Pitstop2. The fluorescence intensity ratio of the GFP^+ over GFP^- cells are shown. Number of embryos analyzed per condition: pCImG/DMSO *n*=2; pCImG/Pitstop2 *n*=4; PAPC-S/DMSO *n*=7; and PAPC-S/Pitstop2 *n*=6. Mean±s.d. (C-F) CDH2 distribution in chicken PSM explants cultured for 4 h in the presence of DMSO (0.2%; C,E; *n*=3) or chlorpromazine (50 µM; D,F; *n*=3). E and F show higher magnifications of the boxed areas in C and D, respectively. t0, last formed boundary at treatment start. Dorsal view, anterior to the top. Scale bars: 100 µm.

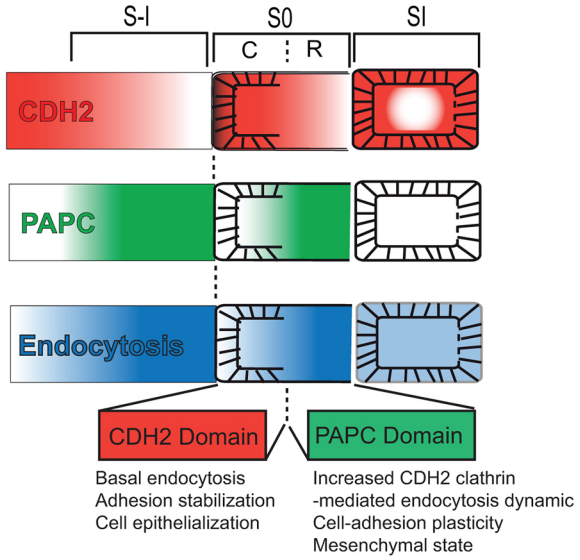

Fig. 8. Model for the role of PAPC in somite segmentation. Segmental expression of PAPC protein (green) is superimposed on the CDH2 adhesion field (red) leading to enhanced endocytosis (blue) clearing locally CDH2 from the cell surface and generating a de-adhesion interface, which allows the formation of a new somitic boundary. C, caudal; R, rostral.

epithelial morphology, as evidenced by the lack of ZO-1 accumulation and failure of tight junction formation (Fig. S5), and displayed a higher level of mislocalized membrane CDH2 (Fig. 7F). These data support the idea that PAPC is involved in the control of CDH2 endocytosis, which is crucial for the formation of the somitic fissure (Fig. 8).

DISCUSSION

How the rhythmic signal of the segmentation clock translates into the activation of a periodic morphogenetic program, ultimately leading to the formation of the epithelial somites is not well understood. Here, we provide evidence for a direct coupling between the segmentation clock oscillator and somite morphogenesis via the periodic regulation of the protocadherin PAPC, which increases the clathrin-mediated endocytosis dynamics of CDH2 to control the formation of the posterior somitic fissure.

We demonstrate that *PAPC* expression in the posterior PSM shows periodic waves of gene expression with similar kinetics to the *LFNG* waves associated to the segmentation clock (Forsberg et al., 1998; McGrew et al., 1998). Blocking Notch signaling pharmacologically in the chicken embryo or genetically in the mouse does not interfere with *PAPC* dynamic expression in the posterior PSM, indicating that this periodic regulation is independent of Notch. In contrast, overexpressing the basic helix-loop-helix transcription factor *MESPO* (the homolog of mesogenin 1, a key target of the Wnt pathway in the PSM; Wittler et al., 2007) is sufficient to drive ectopic *PAPC* expression in the mesoderm in the chicken embryo. Together with the *Papc* downregulation observed in the mouse *Wnt3a* mutant (*Vt*), our work suggests that *PAPC* acts downstream of the Wnt signaling pathway in the posterior PSM. In addition, we show that in the posterior PSM, *PAPC* expression is negatively regulated by FGF signaling and exhibits an expression gradient opposite to the FGF gradient. As FGF signaling has been shown to be periodically activated in the posterior PSM in mouse and chicken embryos (Dale et al., 2006; Dequeant et al., 2006; Krol et al., 2011; Niwa et al., 2007), this argues that *PAPC* is periodically repressed by FGF signaling. Thus, our data indicate that *PAPC* is a novel cyclic gene, positively regulated by Wnt signaling and periodically repressed by FGF signaling in the posterior PSM of chicken embryos.

PAPC expression has been described in the anterior PSM of fish, frog and mouse embryos where it is expressed as dynamic stripes (Kim et al., 2000; Rhee et al., 2003; Yamamoto et al., 1998). Here, we show that Notch inhibition prevents the formation of *PAPC* stripes in the anterior PSM. Importantly, in mouse, *Papc* expression is lost in the *Mesp2*$^{-/-}$ mutant (Nomura-Kitabayashi et al., 2002; Rhee et al., 2003) whereas in frog and chicken embryos overexpression of the *Mesp2* homologs leads to ectopic activation of *PAPC* (Kim et al., 2000). Furthermore, *PAPC* expression in the anterior PSM tightly overlaps with the *Mesp2* stripes. Together, these data show that *PAPC* is a conserved target of the Mesp2 transcription factor and acts downstream of Notch signaling in the anterior PSM in vertebrates.

Our data suggest that, in the chicken embryo, PAPC prevents epithelialization of cells in the rostral somite compartment by controlling CDH2 endocytosis, thus negatively regulating its function. This results in a sawtooth pattern of CDH2 resembling that recently described in zebrafish (McMillen et al., 2016). The

Development (2017) 144, 664-676 doi:10.1242/dev.143974

action of PAPC on CDH2 endocytosis leads to the establishment of an interface between cells expressing high levels of CDH2 (posterior S0) and lower CDH2 levels (anterior S-I) at their cell membrane at the forming somite border. In zebrafish, CDH2 inhibits Integrin alpha5 activation in adjacent PSM and such an interface is required to allow the activation of Integrin alpha5 by the EphA4-Ephrin-B2 system (Julich et al., 2009; Koshida et al., 2005; McMillen et al., 2016). Integrin activation at this interface results in the local assembly of fibronectin fibrils in the forming intersomitic fissure. Our results provide a possible mechanism for the establishment of this important interface between the mesenchymal domain of the rostral part of S-I and the epithelial domain of the caudal part of S0. Such an interface could promote the de-adhesion behavior involved in somite boundary formation and the subsequent matrix-filled fissure formation (Fig. 8). However, no somitic defects have been reported in mice mutant for *EphA4*, ephrin B2 or *Papc* (Adams et al., 1999; Dottori et al., 1998; Yamamoto et al., 2000), whereas in zebrafish, Papc and EphA4 were shown to act through independent mechanisms (Barrios et al., 2003), supporting some level of functional redundancy among the different pathways involved in somite boundary formation.

Several studies suggest that PAPC indirectly controls cell adhesion by negatively regulating the function of classical cadherins (Chen and Gumbiner, 2006; Chen et al., 2009; Yasuda et al., 2007). CDH2 is a major component of adherens junctions and has been implicated in somite morphogenesis (Duband et al., 1987; Horikawa et al., 1999; Linask et al., 1998; Radice et al., 1997). Our study demonstrates that PAPC and CDH2 colocalize at cell-cell junctions and also in trafficking vesicles in the anterior compartment of the forming somites. Remarkably, where the two proteins are co-expressed, CDH2 appears to be abundant in the cytoplasm of the cells and at loose cell-cell connections, whereas, in domains lacking PAPC expression, such as the caudal domain of the forming somite, CDH2 essentially localizes at the cell membrane. Moreover, cells overexpressing PAPC in the anterior PSM lose their epithelial structure and downregulate CDH2 expression at the cell membrane. PAPC overexpression resulted in a striking cell-sorting phenotype and a disruption of normal boundary formation, consistent with a modulation of the CDH2-dependent adhesion of overexpressing cells in the anterior PSM. CDH2 overexpression also results in expressing cells adopting an epithelial fate. This effect can be partly rescued by overexpressing PAPC together with CDH2, supporting the idea that PAPC antagonizes CDH2 function in the anterior PSM. Importantly, the half-life of cadherins is around 5-10 h (Kowalczyk and Nanes, 2012), and thus, given the short timing of fissure formation (less than 2 h in vertebrates), transcriptional regulation of CDH2 would not be able to control CDH2 dynamics in somite formation. Endocytosis has been shown to modulate the adhesive properties of cadherins on short timescales (Kowalczyk and Nanes, 2012; Troyanovsky et al., 2006), leading us to hypothesize that the fast transcriptional dynamic expression of PAPC downstream of the clock signals could regulate CDH2 localization on the short timescale (through endocytosis) required for fissure formation. Interestingly, in the nervous system, PAPC (also known as arcadlin) has been shown to directly trigger CDH2 endocytosis through a p38 MAPK activation, leading to dendrite remodeling (Yasuda et al., 2007). Our results also show that clathrin-mediated endocytosis is active in the anterior PSM and becomes overactivated in PAPC-electroporated cells. Together, these observations support a model in which PAPC antagonizes CDH2 function in the rostral part of the forming somite by promoting its endocytosis. As a result, cells of the rostral compartment of the somite S-I remain mesenchymal, whereas cells of the caudal compartment of the somite S0 form an epithelial posterior wall. This interface will form the posterior somitic fissure (Fig. 8). Although the PSM exhibits an overall uniformly graded distribution of CDH2 in the anterior PSM, our work suggest that the periodic regulation of CDH2 trafficking mediated by PAPC downstream of the segmentation clock triggers local de-adhesion, creating the interface forming the somitic fissure (Fig. 8). Thus, PAPC functions as a morphogenetic translator of the input of the clock and wavefront system, leading to periodic somite boundary formation.

MATERIALS AND METHODS

Embryos

Chicken embryos were staged by days of incubation (e.g. E1, E2) by counting somite pairs and according to Hamburger and Hamilton (HH) (Hamburger, 1992). Wild-type mouse embryos were harvested from timed-mated CD1 mice. *Rbpj*$^{-/-}$, *Raldh2*$^{-/-}$ and *Wnt3a* hypomorph *Vt/Vt* mutant mouse embryos were obtained by conventional breeding of each line. Embryos were genotyped and phenotyped as described (Greco et al., 1996; Niederreither et al., 1999; Oka et al., 1995). Chicken embryo explants were cultured as described (Delfini et al., 2005) in presence of DAPT (10 µM, Calbiochem) (Dale et al., 2003), or SU5402 (80-100 µM, Pfizer) (Delfini et al., 2005), dissolved in DMSO.

PAPC isoform isolation and *in situ* hybridization (ISH)

PAPC full-length sequence was amplified by PCR from cDNA of E2 chicken embryos. A short isoform (*PAPC-S*; Genbank JN252709) and a long isoform (*PAPC-L*; Genbank EF175382) were identified. Sequence alignments were performed using Vector NTI (Informax). Whole-mount ISH was performed as described (Henrique et al., 1995). Chicken *PAPC* probe was synthesized from ChEST435l18. The chicken *LFNG* (Dale et al., 2003) and the mouse *PAPC* (Rhee et al., 2003) probes have been described. Chicken N-cadherin (*CDH2*) probe was amplified by PCR from cDNA using the chicken coding sequence (NM001001615).

Generation of PAPC antibodies and western blot analysis

cDNA coding for fragments of the extracellular domain of chicken PAPC and mouse PAPC were cloned in the pET vector expression system (Novagen), expressed in *Escherichia coli*, purified with a His-Bind Kit (Novagen) and used to immunize rabbits (Cocalico Biologicals). The sera were collected, assayed and validated by western blot and used as anti-PAPC polyclonal antibodies. Western blot analysis was performed following standard procedures (Delfini et al., 2005). Protein extracts were obtained by lysis in RIPA buffer of pools of dissected tissue of E2-E3 chicken embryos after electroporation. The signal was detected with a horseradish peroxidase-conjugated anti-rabbit IgG (1:1000; SouthernBiotech, 4030-05) and an ECL+ kit (Amersham).

Plasmids and *in ovo* electroporation

In ovo electroporations were performed as described (Delfini et al., 2005). Full-length coding sequences of chicken *MESO2* (Buchberger et al., 2002) and *MESPO* (Buchberger et al., 2000) were cloned in pCIG (Megason and McMahon, 2002). The coding sequence of *PAPC-S* was subcloned in pCImG (pCAGGS-IRES-membrane GFP). PAPC RNAi targeting sequences were designed using Genscript and cloned into the RNA interference vector pRFP-RNAi containing an RFP reporter (Das et al., 2006). pBIC (pBI-Cherry) was generated from the Tet-inducible bi-directional promoter pBI (Clontech) by subcloning mCherry in pBI. pBIC-*CDH2* (pBICN) was then generated by subcloning the coding sequence of chicken *CDH2* into pBIC. pBIC-*CDH2* was co-electroporated with pCAGGS-rtTA, and doxycycline (1 µg ml^{-1}) was added *in ovo* after overnight incubation and embryos were re-incubated for a further 7-10 h before fixation. Control embryos were electroporated with matched empty

Development (2017) 144, 664-676 doi:10.1242/dev.143974

vectors, namely pCIG, pCImG, pRFP or pBIC. After electroporation, embryos were re-incubated for 25-30 h. Embryos were then fixed and fluorescent reporter expression was analyzed before ISH and immunohistochemistry processing.

Immunohistochemistry and electron microscopy

Whole-mount immunohistochemistry was performed essentially as described (Bessho et al., 2003). Further details on immunohistochemistry on cryosections and imaging analysis are provided in supplementary Materials and Methods.

PAPC-CDH2 colocalization measurement

Signal intensity and distribution for CDH2, PAPC and F-actin (Phalloidin) were analyzed on immunostained parasagittal chicken embryo sections both at the tissue level (PSM areas) and subcellular level (cell-cell junctions). PSM area signals colocalization analysis was performed using ImageJ (n=3 embryos) to calculate a Pearson's coefficient (ranging from −1 to 1, with 1 corresponding to a total positive correlation between signals). For junction level colocalization analysis, signals along junctions (n=20 junctions) were cross-correlated using IGORPro software (Munjal et al., 2015). A peak centered at 0 µm means that both signals are colocalized. Further details on signal colocalization analysis are provided in supplementary Materials and Methods.

Phenotype quantifications

The distribution of electroporated cells was quantified on confocal images of parasagittal sections of the last three formed somites in at least six embryos per condition. Rostrocaudal distribution corresponds to localization of electroporated cells in the rostral versus the caudal somitic compartments. The mesenchymal index corresponds to the ratio between the mesenchymal versus epithelial fraction of the cells by direct scoring of each cells' location within the somite and polarization based on F-actin, CDH2 and fluorescent reporter expressions. The tissue cell-cell connectivity index corresponds to the average length of cell-cell contact per cell, quantified on electron micrographs using ImageJ. Data are represented normalized to the control S0 caudal domain value, fixed at 100. Statistical significance was assessed using Student's t-test. Further details on phenotypical quantifications are provided in supplementary Materials and Methods.

Endocytosis assays

For the dextran uptake assay, chicken embryos were electroporated with pCImG-PAPC-S or pCImG at stage 5HH then cultured on filter paper on agar/albumen plate (Chapman et al., 2001) for 24 h. Embryos were then treated for 20 min with DMSO or the clathrin-mediated endocytosis inhibitor Pitstop2 (30 µM, Abcam). Next, a sagittal slit was generated within the PSM and embryos were incubated with an Alexa Fluor 647-conjugated dextran (10,000 MW, Molecular probes) for 7 min at 37°C. Embryos were washed in cold PBS before processing with immunostaining for CDH2 and mGFP. Analyses were performed with ImageJ (>110 cells per conditions). For chlorpromazine treatment, bisected posterior embryo explants were cultured for 3-5 h as described (Delfini et al., 2005), the left side treated with DMSO (control) and the right side with chlorpromazine at 50 µM (Sigma). Three embryos per conditions were analyzed. Further details on the endocytosis assays and analysis are provided in supplementary Materials and Methods.

Acknowledgements

We thank Jennifer Pace, Leif Kennedy, Merry McLaird and Barbara Brede for excellent technical help; members of the Pourquié laboratory for helpful discussions; Alexis Hubaud for critical reading of the manuscript; the Stowers Institute Core Centers, Fengli Guo (Stowers) and Yannick Schwab (IGBMC) for electron microscopy; Joanne Chatfield for manuscript editing; Silvia Esteban for artwork; and T. Honjo, P. Chambon and S.A. Camper for providing the *Rbpj*, *Raldh2*, *Vt* mice, respectively.

Competing interests

The authors declare no competing or financial interests.

Author contributions

J.C. initiated, designed and performed most of the experiments and analyzed data. C.G. performed and analyzed the immunocolocalization and endocytosis assays. O. P. supervised the overall project. J.C., C.G. and O.P. performed the final data analysis and wrote the manuscript.

Funding

This work was supported by the Stowers Institute for Medical Research and the Howard Hughes Medical Institute. This work has been partly supported by a National Institutes of Health grant (R01 HD043158 to O.P.), an advanced grant from the European Research Council (ERC-2009-AdG 249931 to O.P.) and a postdoctoral fellowship from the European Molecular Biology Organization (ALTF 406-2015) and Marie Skłodowska-Curie Actions (LTFCOFUND2013) (to C.G.). Deposited in PMC for release after 6 months.

Supplementary information

Supplementary information available online at
http://dev.biologists.org/lookup/doi/10.1242/dev.143974.supplemental

References

Adams, R. H., Wilkinson, G. A., Weiss, C., Diella, F., Gale, N. W., Deutsch, U., Risau, W. and Klein, R. (1999). Roles of ephrinB ligands and EphB receptors in cardiovascular development: demarcation of arterial/venous domains, vascular morphogenesis, and sprouting angiogenesis. *Genes Dev.* **13**, 295-306.

Aulehla, A., Wehrle, C., Brand-Saberi, B., Kemler, R., Gossler, A., Kanzler, B. and Herrmann, B. G. (2003). Wnt3a plays a major role in the segmentation clock controlling somitogenesis. *Dev. Cell* **4**, 395-406.

Barnes, G. L., Alexander, P. G., Hsu, C. W., Mariani, B. D. and Tuan, R. S. (1997). Cloning and characterization of chicken Paraxis: a regulator of paraxial mesoderm development and somite formation. *Dev. Biol.* **189**, 95-111.

Barrios, A., Poole, R. J., Durbin, L., Brennan, C., Holder, N. and Wilson, S. W. (2003). Eph/Ephrin signaling regulates the mesenchymal-to-epithelial transition of the paraxial mesoderm during somite morphogenesis. *Curr. Biol.* **13**, 1571-1582.

Bessho, Y., Hirata, H., Masamizu, Y. and Kageyama, R. (2003). Periodic repression by the bHLH factor Hes7 is an essential mechanism for the somite segmentation clock. *Genes Dev.* **17**, 1451-1456.

Buchberger, A., Bonneick, S. and Arnold, H.-H. (2000). Expression of the novel basic-helix-loop-helix transcription factor cMespo in presomitic mesoderm of chicken embryos. *Mech. Dev.* **97**, 223-226.

Buchberger, A., Bonneick, S., Klein, C. and Arnold, H.-H. (2002). Dynamic expression of chicken cMeso2 in segmental plate and somites. *Dev. Dyn.* **223**, 108-118.

Chal, J. and Pourquie, O. (2009). Patterning and differentiation of the vertebrate spine. *Cold Spring Harbor Monograph The Skeletal System* **53**, 41-116.

Chapman, S. C., Collignon, J., Schoenwolf, G. C. and Lumsden, A. (2001). Improved method for chick whole-embryo culture using a filter paper carrier. *Dev. Dyn.* **220**, 284-289.

Chen, X. and Gumbiner, B. M. (2006). Paraxial protocadherin mediates cell sorting and tissue morphogenesis by regulating C-cadherin adhesion activity. *J. Cell Biol.* **174**, 301-313.

Chen, X., Koh, E., Yoder, M. and Gumbiner, B. M. (2009). A protocadherin-cadherin-FLRT3 complex controls cell adhesion and morphogenesis. *PLoS ONE* **4**, e8411.

Dale, J. K., Maroto, M., Dequeant, M.-L., Malapert, P., McGrew, M. and Pourquie, O. (2003). Periodic Notch inhibition by Lunatic Fringe underlies the chick segmentation clock. *Nature* **421**, 275-278.

Dale, J. K., Malapert, P., Chal, J., Vilhais-Neto, G., Maroto, M., Johnson, T., Jayasinghe, S., Trainor, P., Herrmann, B. and Pourquié, O. (2006). Oscillations of the snail genes in the presomitic mesoderm coordinate segmental patterning and morphogenesis in vertebrate somitogenesis. *Dev. Cell* **10**, 355-366.

Das, R. M., Van Hateren, N. J., Howell, G. R., Farrell, E. R., Bangs, F. K., Porteous, V. C., Manning, E. M., McGrew, M. J., Ohyama, K., Sacco, M. A. et al. (2006). A robust system for RNA interference in the chicken using a modified microRNA operon. *Dev. Biol.* **294**, 554-563.

Delfini, M.-C., Dubrulle, J., Malapert, P., Chal, J. and Pourquie, O. (2005). Control of the segmentation process by graded MAPK/ERK activation in the chick embryo. *Proc. Natl. Acad. Sci. USA* **102**, 11343-11348.

Delva, E. and Kowalczyk, A. P. (2009). Regulation of cadherin trafficking. *Traffic* **10**, 259-267.

Dequeant, M.-L., Glynn, E., Gaudenz, K., Wahl, M., Chen, J., Mushegian, A. and Pourquie, O. (2006). A complex oscillating network of signaling genes underlies the mouse segmentation clock. *Science* **314**, 1595-1598.

Diez del Corral, R. and Storey, K. G. (2004). Opposing FGF and retinoid pathways: a signalling switch that controls differentiation and patterning onset in the extending vertebrate body axis. *Bioessays* **26**, 857-869.

Diez del Corral, R., Olivera-Martinez, I., Goriely, A., Gale, E., Maden, M. and Storey, K. (2003). Opposing FGF and retinoid pathways control ventral neural

pattern, neuronal differentiation, and segmentation during body axis extension. *Neuron* **40**, 65-79.
Dottori, M., Hartley, L., Galea, M., Paxinos, G., Polizzotto, M., Kilpatrick, T., Bartlett, P. F., Murphy, M., Kontgen, F. and Boyd, A. W. (1998). EphA4 (Sek1) receptor tyrosine kinase is required for the development of the corticospinal tract. *Proc. Natl. Acad. Sci. USA* **95**, 13248-13253.
Duband, J. L., Dufour, S., Hatta, K., Takeichi, M., Edelman, G. M. and Thiery, J. P. (1987). Adhesion molecules during somitogenesis in the avian embryo. *J. Cell Biol.* **104**, 1361-1374.
Dubrulle, J., McGrew, M. J. and Pourquié, O. (2001). FGF signaling controls somite boundary position and regulates segmentation clock control of spatiotemporal Hox gene activation. *Cell* **106**, 219-232.
Forsberg, H., Crozet, F. and Brown, N. A. (1998). Waves of mouse Lunatic fringe expression, in four-hour cycles at two-hour intervals, precede somite boundary formation. *Curr. Biol.* **8**, 1027-1030.
Greco, T. L., Takada, S., Newhouse, M. M., McMahon, J. A., McMahon, A. P. and Camper, S. A. (1996). Analysis of the vestigial tail mutation demonstrates that Wnt-3a gene dosage regulates mouse axial development. *Genes Dev.* **10**, 313-324.
Hamburger, V. (1992). The stage series of the chick embryo [comment]. *Dev. Dyn.* **195**, 273-275.
Henrique, D., Adam, J., Myat, A., Chitnis, A., Lewis, J. and Ish-Horowicz, D. (1995). Expression of a Delta homologue in prospective neurons in the chick. *Nature* **375**, 787-790.
Horikawa, K., Radice, G., Takeichi, M. and Chisaka, O. (1999). Adhesive subdivisions intrinsic to the epithelial somites. *Dev. Biol.* **215**, 182-189.
Hubaud, A. and Pourquié, O. (2014). Signalling dynamics in vertebrate segmentation. *Nat. Rev. Mol. Cell Biol.* **15**, 709-721.
Hukriede, N. A., Tsang, T. E., Habas, R., Khoo, P.-L., Steiner, K., Weeks, D. L., Tam, P. P. L. and Dawid, I. B. (2003). Conserved requirement of Lim1 function for cell movements during gastrulation. *Dev. Cell* **4**, 83-94.
Julich, D., Mould, A. P., Koper, E. and Holley, S. A. (2009). Control of extracellular matrix assembly along tissue boundaries via Integrin and Eph/Ephrin signaling. *Development* **136**, 2913-2921.
Julich, D., Cobb, G., Melo, A. M., McMillen, P., Lawton, A. K., Mochrie, S. G. J., Rhoades, E. and Holley, S. A. (2015). Cross-scale integrin regulation organizes ECM and tissue topology. *Dev. Cell* **34**, 33-44.
Kim, S. H., Yamamoto, A., Bouwmeester, T., Agius, E. and Robertis, E. M. (1998). The role of paraxial protocadherin in selective adhesion and cell movements of the mesoderm during Xenopus gastrulation. *Development* **125**, 4681-4690.
Kim, S.-H., Jen, W.-C., De Robertis, E. M. and Kintner, C. (2000). The protocadherin PAPC establishes segmental boundaries during somitogenesis in xenopus embryos. *Curr. Biol.* **10**, 821-830.
Koshida, S., Kishimoto, Y., Ustumi, H., Shimizu, T., Furutani-Seiki, M., Kondoh, H. and Takada, S. (2005). Integrinalpha5-dependent fibronectin accumulation for maintenance of somite boundaries in zebrafish embryos. *Dev. Cell* **8**, 587-598.
Kowalczyk, A. P. and Nanes, B. A. (2012). Adherens junction turnover: regulating adhesion through cadherin endocytosis, degradation, and recycling. *Subcell. Biochem.* **60**, 197-222.
Kraft, B., Berger, C. D., Wallkamm, V., Steinbeisser, H. and Wedlich, D. (2012). Wnt-11 and Fz7 reduce cell adhesion in convergent extension by sequestration of PAPC and C-cadherin. *J. Cell Biol.* **198**, 695-709.
Krol, A. J., Roellig, D., Dequeant, M.-L., Tassy, O., Glynn, E., Hattem, G., Mushegian, A., Oates, A. C. and Pourquie, O. (2011). Evolutionary plasticity of segmentation clock networks. *Development* **138**, 2783-2792.
Kulesa, P. M. and Fraser, S. E. (2002). Cell dynamics during somite boundary formation revealed by time-lapse analysis. *Science* **298**, 991-995.
Linask, K. K., Ludwig, C., Han, M.-D., Liu, X., Radice, G. L. and Knudsen, K. A. (1998). N-cadherin/catenin-mediated morphoregulation of somite formation. *Dev. Biol.* **202**, 85-102.
Luu, O., Damm, E. W., Parent, S. E., Barua, D., Smith, T. H. L., Wen, J. W. H., Lepage, S. E., Nagel, M., Ibrahim-Gawel, H., Huang, Y. et al. (2015). PAPC mediates self/non-self-distinction during Snail1-dependent tissue separation. *J. Cell Biol.* **208**, 839-856.
Makarenkova, H., Sugiura, H., Yamagata, K. and Owens, G. (2005). Alternatively spliced variants of protocadherin 8 exhibit distinct patterns of expression during mouse development. *Biochim. Biophys. Acta* **1681**, 150-156.
Martins, G. G., Rifes, P., Amândio, R., Rodrigues, G., Palmeirim, I. and Thorsteinsdóttir, S. (2009). Dynamic 3D cell rearrangements guided by a fibronectin matrix underlie somitogenesis. *PLoS ONE* **4**, e7429.
McGrew, M. J., Dale, J. K., Fraboulet, S. and Pourquie, O. (1998). The lunatic fringe gene is a target of the molecular clock linked to somite segmentation in avian embryos. *Curr. Biol.* **8**, 979-982.
McMillen, P., Chatti, V., Jülich, D. and Holley, S. A. (2016). A sawtooth pattern of cadherin 2 stability mechanically regulates somite morphogenesis. *Curr. Biol.* **26**, 542-549.
Medina, A., Swain, R. K., Kuerner, K.-M. and Steinbeisser, H. (2004). Xenopus paraxial protocadherin has signaling functions and is involved in tissue separation. *EMBO J.* **23**, 3249-3258.
Megason, S. G. and McMahon, A. P. (2002). A mitogen gradient of dorsal midline Wnts organizes growth in the CNS. *Development* **129**, 2087-2098.
Mohammadi, M., McMahon, G., Sun, L., Tang, C., Hirth, P., Yeh, B. K., Hubbard, S. R. and Schlessinger, J. (1997). Structures of the tyrosine kinase domain of fibroblast growth factor receptor in complex with inhibitors. *Science* **276**, 955-960.
Moreno, T. A. and Kintner, C. (2004). Regulation of segmental patterning by retinoic acid signaling during Xenopus somitogenesis. *Dev. Cell* **6**, 205-218.
Morimoto, M., Takahashi, Y., Endo, M. and Saga, Y. (2005). The Mesp2 transcription factor establishes segmental borders by suppressing Notch activity. *Nature* **435**, 354-359.
Munjal, A., Philippe, J.-M., Munro, E. and Lecuit, T. (2015). A self-organized biomechanical network drives shape changes during tissue morphogenesis. *Nature* **524**, 351-355.
Nakajima, Y., Morimoto, M., Takahashi, Y., Koseki, H. and Saga, Y. (2006). Identification of Epha4 enhancer required for segmental expression and the regulation by Mesp2. *Development* **133**, 2517-2525.
Nakaya, Y., Kuroda, S., Katagiri, Y. T., Kaibuchi, K. and Takahashi, Y. (2004). Mesenchymal-epithelial transition during somitic segmentation is regulated by differential roles of Cdc42 and Rac1. *Dev. Cell* **7**, 425-438.
Niederreither, K. and Dolle, P. (2008). Retinoic acid in development: towards an integrated view. *Nat. Rev. Genet.* **9**, 541-553.
Niederreither, K., Subbarayan, V., Dolle, P. and Chambon, P. (1999). Embryonic retinoic acid synthesis is essential for early mouse post-implantation development. *Nat. Genet.* **21**, 444-448.
Nieto, M. A. (2002). The snail superfamily of zinc-finger transcription factors. *Nat. Rev. Mol. Cell Biol.* **3**, 155-166.
Niwa, Y., Masamizu, Y., Liu, T., Nakayama, R., Deng, C.-X. and Kageyama, R. (2007). The initiation and propagation of Hes7 oscillation are cooperatively regulated by Fgf and notch signaling in the somite segmentation clock. *Dev. Cell* **13**, 298-304.
Nomura-Kitabayashi, A., Takahashi, Y., Kitajima, S., Inoue, T., Takeda, H. and Saga, Y. (2002). Hypomorphic Mesp allele distinguishes establishment of rostrocaudal polarity and segment border formation in somitogenesis. *Development* **129**, 2473-2481.
Oginuma, M., Niwa, Y., Chapman, D. L. and Saga, Y. (2008). Mesp2 and Tbx6 cooperatively create periodic patterns coupled with the clock machinery during mouse somitogenesis. *Development* **135**, 2555-2562.
Oka, C., Nakano, T., Wakeham, A., de la Pompa, J. L., Mori, C., Sakai, T., Okazaki, S., Kawaichi, M., Shiota, K., Mak, T. W. et al. (1995). Disruption of the mouse RBP-J kappa gene results in early embryonic death. *Development* **121**, 3291-3301.
Pourquie, O. and Tam, P. P. L. (2001). A nomenclature for prospective somites and phases of cyclic gene expression in the presomitic mesoderm. *Dev. Cell* **1**, 619-620.
Radice, G. L., Rayburn, H., Matsunami, H., Knudsen, K. A., Takeichi, M. and Hynes, R. O. (1997). Developmental defects in mouse embryos lacking N-cadherin. *Dev. Biol.* **181**, 64-78.
Rhee, J., Takahashi, Y., Saga, Y., Wilson-Rawls, J. and Rawls, A. (2003). The protocadherin Papc is involved in the organization of the epithelium along the segmental border during mouse somitogenesis. *Dev. Biol.* **254**, 248-261.
Saga, Y. (2012). The mechanism of somite formation in mice. *Curr. Opin. Genet. Dev.* **22**, 331-338.
Sawada, A., Shinya, M., Jiang, Y. J., Kawakami, A., Kuroiwa, A. and Takeda, H. (2001). Fgf/MAPK signalling is a crucial positional cue in somite boundary formation. *Development* **128**, 4873-4880.
Sosic, D., Brand-Saberi, B., Schmidt, C., Christ, B. and Olson, E. N. (1997). Regulation of paraxis expression and somite formation by ectoderm- and neural tube-derived signals. *Dev. Biol.* **185**, 229-243.
Takahashi, J. S., Hong, H.-K., Ko, C. H. and McDearmon, E. L. (2008). The genetics of mammalian circadian order and disorder: implications for physiology and disease. *Nat. Rev. Genet.* **9**, 764-775.
Troyanovsky, R. B., Sokolov, E. P. and Troyanovsky, S. M. (2006). Endocytosis of cadherin from intracellular junctions is the driving force for cadherin adhesive dimer disassembly. *Mol. Biol. Cell* **17**, 3484-3493.
Unterseher, F., Hefele, J. A., Giehl, K., De Robertis, E. M., Wedlich, D. and Schambony, A. (2004). Paraxial protocadherin coordinates cell polarity during convergent extension via Rho A and JNK. *EMBO J.* **23**, 3259-3269.
Vermot, J., Llamas, J. G., Fraulob, V., Niederreither, K., Chambon, P. and Dolle, P. (2005). Retinoic acid controls the bilateral symmetry of somite formation in the mouse embryo. *Science* **308**, 563-566.
Watanabe, T. and Takahashi, Y. (2010). Tissue morphogenesis coupled with cell shape changes. *Curr. Opin. Genet. Dev.* **20**, 443-447.
Watanabe, T., Sato, Y., Saito, D., Tadokoro, R. and Takahashi, Y. (2009). EphrinB2 coordinates the formation of a morphological boundary and cell epithelialization during somite segmentation. *Proc. Natl. Acad. Sci. USA* **106**, 7467-7472.
Wittler, L., Shin, E.-H., Grote, P., Kispert, A., Beckers, A., Gossler, A., Werber, M. and Herrmann, B. G. (2007). Expression of Msgn1 in the presomitic

Development (2017) 144, 664-676 doi:10.1242/dev.143974

mesoderm is controlled by synergism of WNT signalling and Tbx6. *EMBO Rep.* **8**, 784-789.

Yamagata, K., Andreasson, K. I., Sugiura, H., Maru, E., Dominique, M., Irie, Y., Miki, N., Hayashi, Y., Yoshioka, M., Kaneko, K. et al. (1999). Arcadlin is a neural activity-regulated cadherin involved in long term potentiation. *J. Biol. Chem.* **274**, 19473-19479.

Yamamoto, A., Amacher, S. L., Kim, S. H., Geissert, D., Kimmel, C. B. and De Robertis, E. M. (1998). Zebrafish paraxial protocadherin is a downstream target of spadetail involved in morphogenesis of gastrula mesoderm. *Development* **125**, 3389-3397.

Yamamoto, A., Kemp, C., Bachiller, D., Geissert, D. and De Robertis, E. M. (2000). Mouse paraxial protocadherin is expressed in trunk mesoderm and is not essential for mouse development. *Genesis* **27**, 49-57.

Yasuda, S., Tanaka, H., Sugiura, H., Okamura, K., Sakaguchi, T., Tran, U., Takemiya, T., Mizoguchi, A., Yagita, Y., Sakurai, T. et al. (2007). Activity-induced protocadherin arcadlin regulates dendritic spine number by triggering N-cadherin endocytosis via TAO2beta and p38 MAP kinases. *Neuron* **56**, 456-471.

Yoon, J. K. and Wold, B. (2000). The bHLH regulator pMesogenin1 is required for maturation and segmentation of paraxial mesoderm. *Genes Dev.* **14**, 3204-3214.